GEOPHYSICS, VOL. 72, NO. 1 (JANUARY-FEBRUARY 2007); P. F25–F34, 11 FIGS., 1 TABLE.
10.1190/1.2400625

Magnetotelluric static shift: Estimation and removal using the cokriging method

Benoit Tournerie[1], Michel Chouteau[2], and Denis Marcotte[2]

ABSTRACT

We present and test a new method to correct for the static shift affecting magnetotelluric (MT) apparent resistivity sounding curves. We use geostatistical analysis of apparent resistivity and phase data for selected periods. For each period, we first estimate and model the experimental variograms and cross variogram between phase and apparent resistivity. We then use the geostatistical model to estimate, by cokriging, the corrected apparent resistivities using the measured phases and apparent resistivities. The static shift factor is obtained as the difference between the logarithm of the corrected and measured apparent resistivities. We retain as final static shift estimates the ones for the period displaying the best correlation with the estimates at all periods. We present a 3D synthetic case study showing that the static shift is retrieved quite precisely when the static shift factors are uniformly distributed around zero. If the static shift distribution has a nonzero mean, we obtained best results when an apparent resistivity data subset can be identified a priori as unaffected by static shift and cokriging is done using only this subset. The method has been successfully tested on the synthetic COPROD-2S2 2D MT data set and on a 3D-survey data set from Las Cañadas Caldera (Tenerife, Canary Islands) severely affected by static shift.

INTRODUCTION

The magnetotelluric (MT) static shift is a galvanic distortion effect that locally shifts apparent resistivity sounding curves by a scaling factor s that is independent of the frequency, keeping the phases unchanged. This effect is caused by charge accumulation at boundaries of shallow conductive heterogeneities, which disturb the regional electric field locally. It is clear that this vertical shift of the apparent resistivity curves can lead to errors in the inverted model because the resistivities and depths of the final model will be scaled by s and $\sqrt{s}$, respectively, for a 1D layered model. Correction for this effect is then of first importance before any interpretation of MT data. The static shift effect and its removal has been studied extensively (e.g., Jones, 1988; Singer, 1992; Ogawa, 2002), and we will present here the main methods that have been proposed to correct the MT resistivity curves.

Spatial filtering of the electric field (see Singer, 1992, for a review) is mainly associated with the electromagnetic array profiling (EMAP) method (Torres-Verdín and Bostick, 1992). In EMAP, the electric field is measured using a large amount of dipoles continuously distributed along the profile. Static shifts are then controlled by low-pass filtering of the electric measurements. Larger dipoles can also be used to reduce the static shift effect (Langlois et al., 1996) An application is presented by Tournerie and Chouteau (1998), who used telephone lines as electric dipoles of approximately 100 km length to remove static shifts on sounding curves to retrieve the deep (mantle) conductivity structure and to define one long-period, regional reference MT curve.

Continuous measurements of MT data along a profile and very long dipoles are not standard in MT surveys. In most MT surveys, sites are separated by some distance (typically from one hundred meters to a few kilometers). Zhang et al. (1995) successfully applied spatial filtering to MT data distributed on a 60-km profile in Abitibi, Canada, to suppress static shifts. Apparent resistivities were first interpolated with a 2-km sampling interval before a fourth-order Butterworth low-pass filter was applied with a cutoff frequency of 0.04 km^{-1}. Another solution to reduce static shifts is spatial averaging of MT data. For example, Berdichevsky et al. (1980) used a geometric average of the effective apparent resistivity ρ_a^{eff} on each of 10 predefined zones of the Baikal region.

The use of other geophysical (or even geologic) information available on the survey area is an alternative to the previous meth-

Manuscript received by the Editor February 24, 2006; revised manuscript received September 19, 2006; published online December 29, 2006.
[1]Formely Ecole Polytechnique, Department of CGM Engineering, Montreal, Quebec, Canada; presently, Quantec Geoscience, 116 Spadina Avenue, Suite 400, Toronto, Ontario M5V 2K6, Canada. E-mail: btournerie@quantecgeoscience.com.
[2]Ecole Polytechnique, Department of CGM Engineering, P.O. Box 6079, Station CV, Montreal, Quebec H3C 3A7, Canada. E-mail: chouteau@geo.polymtl.ca; denis.marcotte@polymtl.ca.

ods. For example, Jones (1988) used borehole information to correct the COPROD data set. The laterolog electrical resistivity section is used to define the subsurface conductivity model to identify one specific layer (named the *key-layer* by Ogawa, 2002) on which 1D models have to correlate. Reference MT curves derived from GDS (Schultz et al., 1993; Bahr, 1988) or static-free MT soundings (Tournerie and Chouteau, 2002) can also be used to correct the apparent resistivity curves of sites from a survey area including sites for which reference curves are available. However, such a priori information is rarely available for any MT survey, or it may cost a substantial amount in the case of the borehole control technique.

The use of a magnetic sounding method such as the transient electromagnetic (TEM) method is increasing. Applications of this method can be found in Andrieux and Wightman (1984), Sternberg et al. (1988), Pellerin and Hohmann (1990), and Zhang et al. (1995). The principal advantage of such methods is that they use the secondary magnetic field to estimate a 1D layered conductivity model at the station up to the depth of penetration of the method. This model may present the real subsurface conductivities and depth of the shallow layers because the magnetic field is not affected by charge accumulation at boundaries of shallow heterogeneities (i.e., no static shift in the data). The MT response of the resulting 1D model is then computed and used as a high-frequency MT reference curve to correct apparent resistivity sounding curves. Meju (1996) integrates these two steps into one by performing a joint inversion of the TEM apparent resistivity and the MT-phase data. However, this interpretation is only possible when MT and TEM data overlap over some depth of penetration. Furthermore, this is only applicable when the size of the conductive heterogeneity causing the static shift is smaller than the transmitter loop. Finally, it is not applicable when the shallow resistivities are high, because the TEM response can often be below the instrumentation noise level.

More recently, Ledo et al. (2002) have developed a relation between the vertical magnetic transfer function (i.e., tipper) and the horizontal gradient of the impedance. Coefficients of the recursive linear equation are proportional to the static shift parameters that can be estimated accordingly to one static-free (or corrected) MT site.

Static shift parameters can also be considered as unknown in the inversion of MT survey data and are to be estimated during inversion for a minimum structure model. This approach is introduced in the widely used 2D Occam (deGroot-Hedlin, 1991) and RRI (Smith and Booker, 1991) inversion programs and is now included in other codes (e.g., RLM, Rodi and Mackie, 2001). Solutions are computed by minimizing an L2 norm with different smoothness criteria and using some assumptions on the distribution (see Ogawa and Uchida, 1996) of the static shift parameters. Another alternative is to run 2D inversion based on the MT-phase data by increasing errors on the apparent resistivities (Wu et al., 1993).

Nevertheless, when MT sites are distributed over a survey area, spatial variations of the sounding results in that the two horizontal directions have to be accounted for. Removal of static shift using the 2D inversion method for minimum structure alone may give inaccurate solutions. In particular, static correction of the transverse electric (TE) apparent resistivity is difficult because the complex impedance Z_{TE} depends on the variation of the electric field oriented perpendicular to the profile caused by small heterogeneities located off line or between lines that are not accounted for when using 2D imaging. On the other hand, static shifts affecting the transverse magnetic (TM) apparent resistivities are generally better determined because the complex impedance Z_{TM} varies with the electric field parallel to the profile and, therefore, orthogonal to the small heterogeneities located along the profile. However, removal of the static shift on sites aligned on a 2D profile is independent of the correction performed on adjacent lines; therefore, correlation of the corrections (i.e., final amplitude of the apparent resistivities) from line to line is not warranted. Such variations may introduce unrealistic lateral variations of the depth and of the conductivities in the 3D model built from the 2D models.

Spatial filtering seems to be the most appropriate solution because this method can be applied easily on 2D apparent resistivity maps. However, the user mainly controls the design of the filter, and results may be very sensitive to the selected input parameters, particularly if no a priori information from unaffected subsets of the data are used to formulate them.

Lateral changes of the subsurface conductivity should cause coincident variations of the apparent resistivity ρ_a and phase ϕ for an appropriate depth of investigation (i.e., for a given period). Apparent resistivities displaying spatial variations (especially with short wavelength) that are not correlated with a similar variation of the phases may indicate that small, near-surface heterogeneities are causing a static shift of the apparent resistivities. The objective is, therefore, to correct ρ_a such that the spatial structures of ρ_a and ϕ are similar. Both are known to be derived from the MT impedance and are related through Hilbert transforms (see Fischer and Schnegg, 1980).

In the following, we propose a technique for static correction based on the similarities of spatial structure of the phases and apparent resistivities. In geostatistics, the cokriging method is used to better estimate a variable (primary) using information from a secondary variable related to the first and for which the spatial structure is better known. We first present some algebra to highlight some characteristics of the complex MT impedance regarding the static shift s. In the sections that follow, we introduce the spatial cokriging method and its application to static shift correction in MT. We use a 3D synthetic data set to illustrate our results on an unbiased and biased uniform distribution of the static shift. Finally, the technique is applied to the COPROD-2S2 (2D) synthetic data set and to a 3D MT survey data set from Tenerife, Canary Islands.

THE MAGNETOTELLURIC IMPEDANCE

We know from magnetotelluric theory (see Orange, 1989; Vozoff, 1991, for a complete review of the method) that the complex MT impedance Z_{mn} can be expressed using the apparent resistivity ρ_a^{mn} and phase ϕ_{mn} as

$$Z_{mn} = (\rho_a^{mn}\mu_0\omega)^{1/2}\exp[j\phi_{mn}], \qquad (1)$$

where m and n can be both x and y, the directions of measurement, $j = \sqrt{-1}$, μ_0 is the magnetic permeability of free space, and ω is the angular frequency ($\omega = 2\pi f$, with f the frequency).

One can then define a complex variable z (omitting the m and n terms) by

$$z = \log(Z) - 0.5\log(\mu_0\omega) = 0.5\log(\rho_a) + j\phi \qquad (2)$$

that simplifies, by using $r_a = \log(\rho_a)$, to

$$z = 0.5r_a + j\phi. \qquad (3)$$

For each period T, we estimate

$$z(x,y) = 0.5r_a^{\text{obs}}(x,y) + j\phi^{\text{obs}}(x,y), \tag{4}$$

where obs is for observed. Because of the static shift that can be present at each site,

$$r_a^{\text{obs}} = r_a^{\text{true}} + s + \epsilon_r, \tag{5}$$

where s is the logarithm of the static shift affecting locally the apparent resistivity (s is independent of r_a^{true}), and $\epsilon_r$is the error on the r_a^{obs} determination.

The static shift affects only the real part r_a of the modified complex impedance z (see equations 4 and 5). Phases, i.e., the imaginary part of z, are not altered by this distortion. Then, removal of the static shift effect at one site may be viewed as getting a better estimate of the real part of the modified complex impedance z, i.e., r_a. Lajaunie and Béjaoui (1991) and Wackernagel (2003) demonstrate that a better estimation of the complex variable z ($z = u + jv$) may be obtained by cokriging the real (u) and the imaginary (v) part of z, in comparison to the separate kriging of u and v or the complex kriging of z.

THE COKRIGING METHOD

Cokriging is an interpolation and extrapolation method developed for the evaluation of mining resources but is now widely applied in other areas of earth sciences (see Nyquist et al., 1996, for an application to seismic interpretation). Here, we will briefly introduce the cokriging method; a complete development of the method can be found in Cressie (1993), Chilès and Delfiner (1999), and Wackernagel (2003).

Considering the discrete subset S of the continuous complex function $z(\mathbf{r})$, i.e., $S = \{z(\mathbf{r}_k) = z_k = u_k + jv_k; k = 1, \ldots, n\}$, the linear estimator for a variable z_0, labeled here $\tilde{z}_0$, can be expressed by

$$\tilde{z}_0 = \tilde{u}_0 + j\tilde{v}_0 = \sum_{k=1}^{n} (\mu_{1k}u_k + \eta_{1k}v_k) + j\sum_{k=1}^{n} (\mu_{2k}u_k + \eta_{2k}v_k), \tag{6}$$

where μ_{1k}, μ_{2k}, η_{1k}, and η_{2k} are the weights of the estimator. The real and imaginary part of $\tilde{z}_0$ may be analyzed separately, but they both depend on the real and imaginary part of the z_k terms.

The best linear unbiased estimator (BLUE) for $\tilde{u}_0$ is obtained by minimizing the error $\sigma_e^2 = \text{var}[u_0 - \tilde{u}_0]$; this leads to the resolution, using the Lagrange method, of the system of equations (Lajaunie an Béjaoui, 1991; Wackernagel, 2003):

$$\begin{aligned}
&\sum_{p=1}^{n} \mu_{1p}\text{Cov}(u_k,u_p) + \sum_{p=1}^{n} \eta_{1p}\text{Cov}(u_k,v_p) + \lambda_{1r} \\
&\quad = \text{Cov}(u_0,u_k), \\
&\sum_{p=1}^{n} \mu_{1p}\text{Cov}(v_k,u_p) + \sum_{p=1}^{n} \eta_{1p}\text{Cov}(v_k,v_p) + \lambda_{1i} \\
&\quad = \text{Cov}(u_0,v_k),
\end{aligned} \tag{7}$$

$$\text{with} \sum_{p=1}^{n} \mu_{1p} = 1 \text{ and } \sum_{p=1}^{n} \eta_{1p} = 0; \quad \forall\ k = 1, \ldots, n,$$

where Cov is the covariance function, and λ_{1r} and λ_{1i} are the Lagrange multipliers. (Note that a similar system may be derived for the imaginary part $\tilde{v}_0$.)

In the cokriging system (equation 7), the covariances C_{uv} are defined by

$$C_{uv}(h) = \text{Cov}(u(r),v(r+h)), \tag{8}$$

with r representing the site position, and h is a distance to that site.

The covariance model $C_{uv}(h)$ is estimated from the data. Assuming second-order stationarity, we define the theoretical cross-covariance $C_{uv}(h)$ by

$$C_{uv}(h) = \text{E}\left[(u(r) - \text{m}_u) \cdot (v(r+h) - \text{m}_v)\right], \tag{9}$$

with $\text{m}_u = \text{E}[u(r)]$ and $\text{m}_v = \text{E}[v(r)]$, where $\text{E}[\cdot]$ is the expectation of the function (i.e., m is the mean). Then, assuming symmetry of the cross-covariance [i.e., $C_{uv}(h) = C_{uv}(-h)$], we can use the cross variogram defined by

$$\gamma_{uv}(h) = \frac{1}{2}\text{E}\left[(u(r+h) - u(r)) \cdot (v(r+h) - v(r))\right] \tag{10}$$

to compute the covariance using the relation

$$\gamma_{uv}(h) = C_{uv}(0) - C_{uv}(h). \tag{11}$$

Experimental variograms γ_{uu}^s and γ_{vv}^s and cross-variogram γ_{uv}^s are computed from the data for different classes of distances h of constant width δaccording to

$$\gamma_{uv}^s(\bar{h}) = \frac{1}{2N(h)}\sum_{l=1}^{N(h)} \Delta u(\delta h) \cdot \Delta v(\delta h), \tag{12}$$

with $\Delta u = u(r_l + \delta h) - u(r_l)$, $\Delta v = v(r_l + \delta h) - v(r_l)$, and $\delta h \in [h, h+\delta]$, where $N(h)$ is the number of pairs in the class.

Simple, positive definite models are then used to model those variograms, enabling covariance computation for any separation vector h. The functions used are of the form $c \bmod(a)$, where mod is the variogram model, c is the variance, and a is the range representing the distance at which data are uncorrelated ($C(h>a) = 0$), or nearly uncorrelated. The mod functions currently used are presented in Table 1. However, one needs to combine at least two models (the first model being the Nugget model) to adjust the experimental variogram so that the final model is given by

Table 1. Mathematical expressions for different variogram models; *c* is the variance and *a* is the range (Wackernagel, 2003).

Nugget (Nug)	0 c	$\lvert h\rvert = 0$ $\lvert h\rvert > 0$
Spherical (Sph)	$c\,[1.5\lvert h\rvert/a - 0.5(\lvert h\rvert/a)^3]$ c	$0 < \lvert h\rvert < a$ $\lvert h\rvert \geq a$
Gaussian (Gau)	$c\,[1 - \exp(-(\lvert h\rvert/a)^2)]$	
Exponential (Exp)	$c\,[1 - \exp(-(\lvert h\rvert/a))]$	
Linear (Lin)	$c\,\lvert h\rvert^b$	$0 < b < 2$

$$\gamma(h) = c_0(1 - \delta(h)) + c \operatorname{mod}(a), \tag{13}$$

where $\delta(h)$ is the Kronecker function, and c_0 is called the nugget effect. It aggregates the measurement error variance and the short-scale variability. The quantity $\sigma^2 = c_0 + c$ is the variance of u or v (equal to the sill of γ) (see Figure 1).

APPLICATION TO MT STATIC SHIFT

As the method proceeds from a map of ρ_a and ϕ, the impedance attributes must be selected for a period. Selecting a particular period is not a restriction because the static-shift affects the apparent resistivity sounding curve at all periods in the same manner. Therefore, any period can be used if the data are of high quality. However, the selected period should be such that an EM skin depth is greater than the scale of the heterogeneities causing the static shift so that the static shift becomes period independent. Then, the shortest period that meets this criterion should be used because it will be less sensitive to the broad, lateral conductivity variations that are the survey targets. Rapid changes of ρ_a can then be attributed mostly to static shift caused by shallow heterogeneities.

Having selected maps of ρ_a and ϕ at period T, our first step is the computation of the experimental variograms for the logarithm of the apparent resistivity (i.e., r_a) and for the phase and that of their cross variogram. Here, the distribution of r_a and ϕ are represented by the functions u and v previously introduced.

For most MT surveys, the width of the classes of the experimental variograms (i.e., δ in equation 12) will be defined by the grid spacing of the MT sites, i.e., the minimum distance between the MT stations. However, we will have to increase δ if the number of pairs for the first class is smaller than the total number of sites, simply because that first class may badly represent the variations in the vicinity of all MT sites. That number of pairs depends on the size of the data set and on the distance between the MT stations, but a number close to 50%–100% of the total number of MT sites may be enough to represent the variation of the variable in the neighborhood of the MT sites. Furthermore, a minimum of MT sites is required to compute (and to model) the experimental variogram over 5 to 10 classes. Here again, that number is not well defined and may depend on the distribution of the MT sites (2D line or 3D data set). However, we consider that a number of MT sites close to 30 should allow enough combination of small and large distances so that an experimental variogram can be estimated.

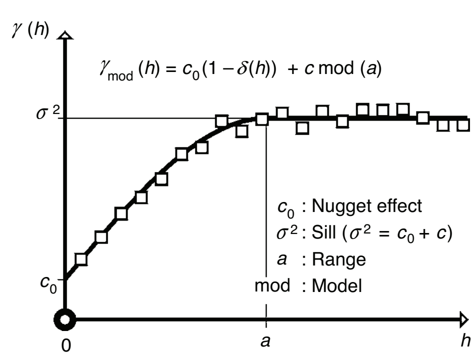

Figure 1. Experimental and modeled variograms displaying c_0, c, and a; $\delta(h)$ is the Kronecker function, and mod represents the model of the variogram (see examples in Table 1).

The second step of the method consists of modeling variograms using simple, positive definite models (equation 13). It is important to note here that the range a of that model is first computed using the phase measurements. This value is then fixed for the other models at that period T. Nugget effects, variances for the variogram model of r_a, and the cross-variogram model between ϕ and r_a are then estimated by minimizing the error between the model and the experimental (cross)variograms.

Here, it should be also noted that the estimation of the range a could be used directly by the spatial filtering method. This parameter represents the distance at which data are uncorrelated or nearly uncorrelated; therefore, it could be input to define the optimal cutoff frequency.

From equations 4, 5, and 11, and assuming that static distortions and measurement errors at two different sites are uncorrelated, we get

$$\begin{aligned}\gamma_{r_a^{\text{obs}},r_a^{\text{obs}}}(h) &= C_{r_a^{\text{obs}},r_a^{\text{obs}}}(0) - C_{r_a^{\text{obs}},r_a^{\text{obs}}}(h)\\ &= \operatorname{Var}(r_a^{\text{true}}) + \operatorname{Var}(s) + \operatorname{Var}(\epsilon_r) - C_{r_a^{\text{true}},r_a^{\text{true}}}(h),\end{aligned} \tag{14a}$$

$$\begin{aligned}\gamma_{\phi^{obs},\phi^{obs}}(h) &= C_{\phi^{\text{obs}},\phi^{\text{obs}}}(0) - C_{\phi^{\text{obs}},\phi^{\text{obs}}}(h)\\ &= \operatorname{Var}(\phi^{\text{true}}) + \operatorname{Var}(\epsilon_\phi) - C_{\phi^{\text{true}},\phi^{\text{true}}}(h),\end{aligned} \tag{14b}$$

$$\begin{aligned}\gamma_{r_a^{obs},\phi^{obs}}(h) &= C_{r_a^{\text{obs}},\phi^{\text{obs}}}(0) - C_{r_a^{\text{obs}},\phi^{\text{obs}}}(h)\\ &= C_{r_a^{\text{true}},\phi^{\text{true}}}(0) + C_{\epsilon_r,\epsilon_\phi}(0) - C_{r_a^{\text{true}},\phi^{\text{true}}}(h).\end{aligned} \tag{14c}$$

It is clear that the variogram of r_a (equation 14a) is discontinuous at the origin unless we have error-free data with no static distortion. The nugget effect depends on the variability of the static shift and the error of the r_a determination. However, the latter is generally much smaller than the former. The variogram of ϕ (equation 14b) shows that the nugget effect will be small if the phase data is well estimated. Finally, the cross-variogram $\gamma_{r_a,\phi}$ (equation 14c) will have no nugget effect if the errors in estimating r_a and ϕ are independent (usually they are not because r_a and ϕ are estimated from the same observed MT data).

Then, cokriged values of the logarithm of the apparent resistivity (r_a^{cok}) are obtained by solving the cokriging system (equation 7) for a subset of sites located close to the MT stations. A small horizontal displacement ε_r (e.g., $\varepsilon_r \approx 10^{-7}$ km) is added to the position of the MT sites r_{obs} because the computed cokriged value is equal, by definition, to the measured value ($r_a^{\text{cok}} = r_a^{\text{obs}}$) when the cokriging point (r_{cok}) is located exactly at an observation point (r_{obs}): the cokriging system (eqaution 7) reproduces the observation.

Finally, because the displacement ε_r is very small, the static-shift factor for each MT site can be defined by the difference between (1) the measured value of the logarithm of the apparent resistivity (r_a^{obs}) at the MT site location and (2) the cokriged value computed at a position close to that MT site:

$$s \equiv r_a^{\text{obs}} - r_a^{\text{cok}} = \log[\rho_a^{\text{obs}}] - \log[\rho_a]^{\text{cok}}. \tag{15}$$

SYNTHETIC EXAMPLES

The model

The synthetic model studied here is presented in Figure 2a. Two faults control the 3D structure of the model. The first fault is normal (parallel to X) with a vertical displacement of 500 m. The second is a transform fault parallel with the Y-axis with a sinistral displacement of 1 km. A first conductive layer (10^2 ohm-m, $h = 100$ m) covers all the area. Then, for the western part of the model (see A in Figure 2b), the model is defined by a resistive layer (10^4 ohm-m, $h = 2$ km) above the semi-infinite conductive layer (10^2 ohm-m). For the eastern part of the model (see B in Figure 2b), there is a thin resistive layer (10^3 ohm-m, $h = 100$ m) overlying a conductive layer (10^2 ohm-m, $h = 300$ m), and then, the resistive layer (10^4 ohm-m, $h = 2$ km) above the semi-infinite conductive layer (10^2 ohm-m).

The MT response of that model is calculated using the 3D forward-modeling code developed by Mackie et al. (1994) for periods ranging from 0.0001 to 1 s. Pseudosections of the XY and YX apparent resistivities and phases are presented in Figure 2c-j. The line labeled pN is located at X = +900 m, and the one labeled pS is at X = −900 m.

We can clearly observe that the main variations in the pseudosections of the apparent resistivities and phases are located between the coordinates −1 km and +1 km along the y-axis. The lateral variation is, however, located in the negative zone of the y-axis ($[-1,0]$) for the pN profile (X = +900 m) and in the positive zone of the y-axis ($[0, +1]$) for the pS profile (X = −900 m). These lateral variations clearly mark the faults parallel to the x-axis, whereas the difference in the y-position marks the transform fault located at X = 0 km.

A subset of regularly spaced MT sites is then selected on an area of 3×3 km^2 centered on the model (see Figure 2a). The grid (site) spacing is 300 m. Static shifts are modeled at each MT site by adding a value s to the logarithm of ρ_a (i.e., r_a), while the phases are kept unchanged. The value of s, therefore, represents the logarithm of the static shift. The level of s is selected randomly from a uniform distribution. The next sections will present our results for the XY mode; we assume a centered ($s \in [-1; +1]$) and biased ($s \in [0; +2]$) distribution of the static shift affecting all or a subset of the MT sites.

For each case, variograms of the phases ϕ and the modified apparent resistivities r_a, and the cross variogram between ϕ and r_a, are computed for each period T. Here, the width δ of the class of the experimental variograms (equation 12) is defined by the grid spacing of the MT sites. The number of pairs for the first class of the experimental variogram is then 132. A Gaussian model is fitted to each variogram:

$$\gamma(h) = c_0(1 - \delta(h)) + c(1 - \exp(-(h/a)^2)). \quad (16)$$

For each period, the range a of this model is first estimated using the phase measurements. This value is then fixed for the other models at that period T. Nugget effects, variances for the variogram model of r_a, and the cross variogram model between ϕ and r_a are then estimat-

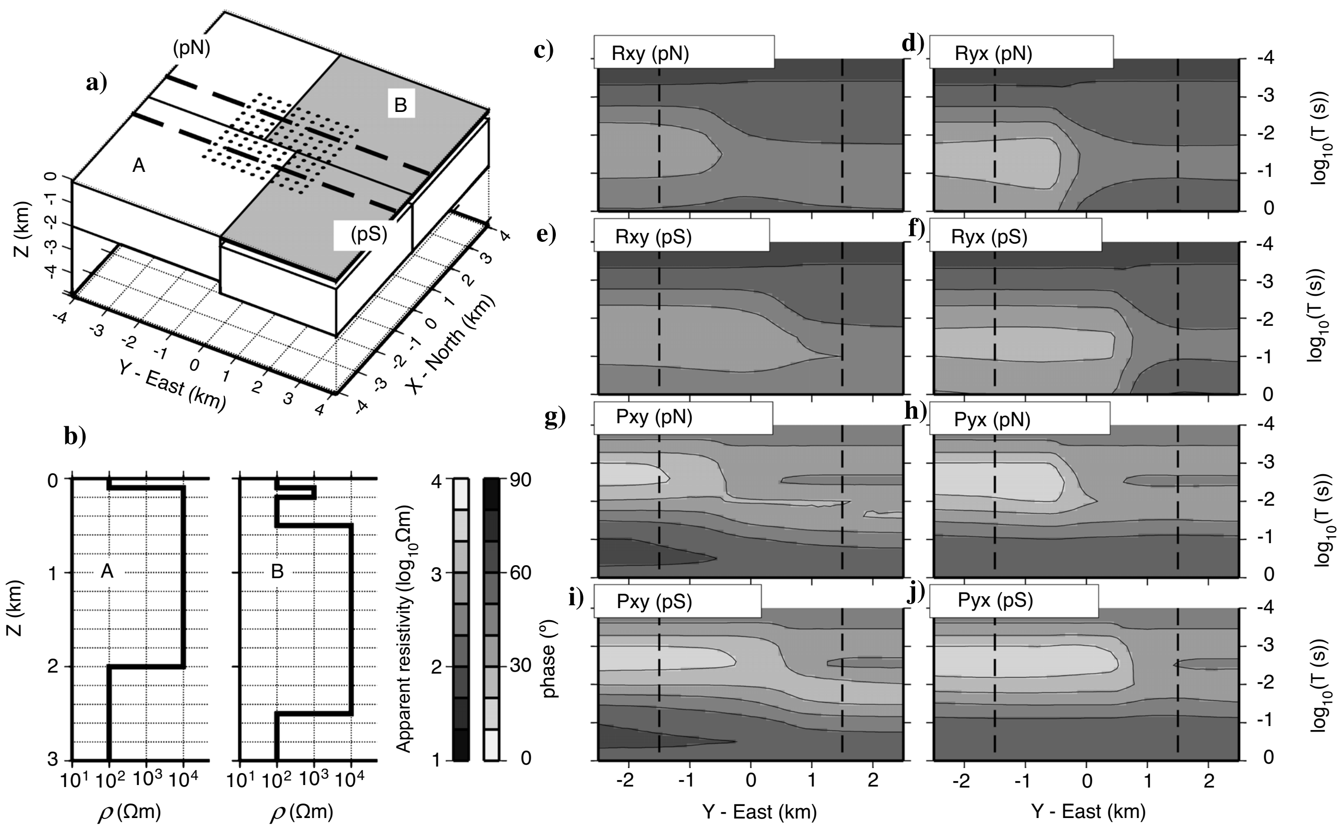

Figure 2. Synthetic model and MT pseudosections: (a) 3D view of the model. Black dots indicate the MT sites used in this study; the black dashed lines are the locations of the profiles (pN and pS) which include the pseudosections shown in (c-j). (b) Resistivity logs for sites A and B [location shown in (a)]; (c-j) Pseudosections at X = +900 m(pN) and X = −900 m (pS) of the modeled MT data. Rxy, Pxy, Ryx, and Pyx are the apparent resistivity R and phase P of modes XY and YX, respectively. The dashed lines on the pseudosections indicate limits of the MT survey.

ed by minimizing the error between the model and the experimental (cross) variograms. Cokriged values r_a^{cok} at each site are then estimated by resolving the cokriging system. This is performed using the cokri2 Matlab program developed by Marcotte (1991). The static shift parameter is finally estimated using equation 15.

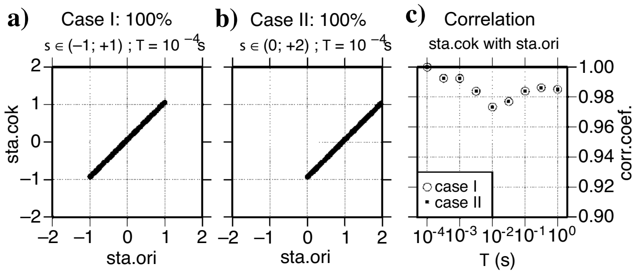

Figure 3. Results for the synthetic cases I and II. (a) Case I: 100% of the MT sites are affected by a static shift $s \in [-1;+1]$. (b) Case II: 100% with $s \in [0;+2]$. Results presented in (a) and (b) are for $T = 10^{-4}$ s. (c) Correlation coefficients between the solution of the static shift estimated at each period and the original (input) static shift.

Case I: 100% of MT sites with $s \in [-1;+1]$

In this case, the static shift affects all sites (100%). Apparent resistivities at all sites were shifted accordingly to a uniform distribution of the static shift, assuming a static-shift value $s \in [-1;+1]$ per site. Results for $T = 10^{-4}$ s are presented in Figure 3a. For this period, there is a good correlation between the original (sta.ori) and the estimated (sta.cok) static-shift factors. The correlation coefficient between sta.cok and sta.ori is R = 0.9999, and the error $S1E$ defined by $\Sigma|\mathrm{sta.cok} - \mathrm{sta.ori}|/N$ is 0.0654 ($S1E_A$).

A static-shift data set $\{SS[k] = \{s_l^k; l = 1, \ldots, N\}; k = 1, \ldots, M\}$ was computed for each period k. Correlations between each data set $SS[k]$ and the original (input) static shift are presented in Figure 3c (circles). The correlation decreases slightly with larger periods, with a minimum found close to period $T = 10^{-2}$ s, which is the period most sensitive to the underlying geological structure as shown by the pseudosections in Figure 2.

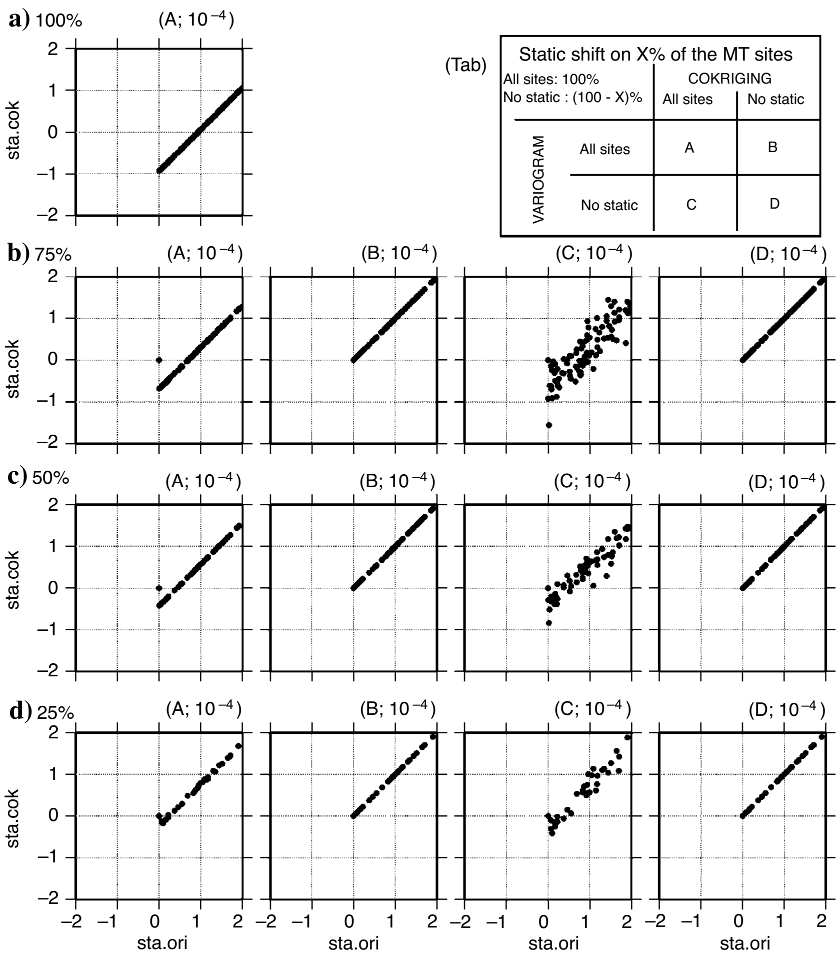

Figure 4. Graphs of the variation of the estimated static shift (sta.cok) versus the original one (sta.ori) for $T = 10^{-4}$ s when $s \in [0;+2]$. The insert table (Tab; top-right) defines the different methods (cases A–D) used to estimate the static shift according to the amount of sites used to compute the experimental variogram of r_a^{obs} and the cokriged values r_a^{cok}. Solutions for different amount of MT sites affected by static shifts (from 100% to 25%) are shown in 4(a-d).

Case II: 100% of MT sites with $s \in [0;+2]$

This case is similar to case I except that a bias has been introduced in the static shift distribution so that now $s \in [0;+2]$. This case represents MT soundings systematically recorded on resistive heterogeneities, for example, topographic highs within a swamp. Results of the estimation of the static shifts are presented in Figure 3b for $T = 10^{-4}$ s. It is clear that results are similar to those previously found in case I. However, it is important to note that the estimator cannot resolve the bias introduced in the original static shift. For example, the error $S1E$ for $T = 10^{-4}$ s now has a value of 0.9345 that corresponds to $1 - S1E_A$.

Removal of that bias can be assessed only by using some additional information to fix the background level for the true apparent resistivity.

Phase measurements are not affected by the static shift effect, so we can use measurements from all the MT sites at the selected period T to compute the experimental variogram for ϕ and to define the range a and the models $\gamma(h)$ of the variograms and the cross variogram.

However, if we can define a particular subset of MT sites that is not affected by static shifts (i.e., $s = 0$ for those MT sites), there are now different alternatives for the estimation of the static shift from the apparent resistivity, depending on the number of MT sites known to be affected by static shifts.

In fact, if we define X as the percentage of MT sites with static shift, then we can compute the experimental variogram of r_a^{obs} using either all the MT sites (i.e., 100%) or using only measurements from the MT sites that are not affected by static shift (i.e., 100% – X%). Similarly, we can use observations from all the MT sites at the selected period T to compute the cokriged values r_a^{cok} or use only the subset of MT data not affected by static shifts. Hence, four different strategies are therefore possible as summarized in the table (tab) insert in Figure 4.

A compilation of the results is presented in Figure 4 where each plot displays the variation of the computed static shift (sta.cok) versus the original (input) static shift (sta.ori) for $T = 10^{-4}$ s. The amount of sites with static shift $s \neq 0$ varies from 100% to 25% (Figure 4a-d). Cases A to D (i.e., columns in Figure 4) represent the different solutions of sta.cok defined by the set of MT sites used to compute (1) the experimental variogram of r_a^{obs} (100% or 100% $- X$%) and (2) the cokriged values r_a^{cok} (100% or 100% $- X$%). Explanation for each case is given in Figure 4. For example, in Figure 4d, case B, 25% of the MT sites are affected by static shift; the experimental variogram for r_a^{obs} is computed using data from all MT sites, but the cokriged values r_a^{cok} are estimated using only those MT sites not affected by static shifts. Correlation between the different solutions $\{SS[k] = \{s_l^k; l = 1, \ldots, N\}; k = 1, \ldots, M\}$ computed at each period T_k and the original (input) static shift are shown in Figure 5.

First, we observe that the worst solution is found in case C, where there is not a good correlation between sta.cok and sta.ori as shown by the dispersion along the expected linear trend between sta.cok and sta.ori. However, even in this case, the bias can approximately be estimated, especially for case C in Figure 4d.

A good correlation is observed in case A for all the periods (see Figure 5), but the estimator cannot recover the bias present in the original static shift data set (Figure 4). Nevertheless, the estimation of the bias is improved with a decreasing amount of sites affected by static shift (case A-a to A-d; 100% to 25%). This case illustrates the situation where all the MT sites are possibly affected by a static shift; therefore, no information is used to constrain the solution.

Best results are found for cases B and D (see Figures 4 and 5). In both cases, the original bias has been well estimated and there is a good correlation between sta.cok and sta.ori for all the periods (Figure 5). It is evident here that the static shift is well estimated because only static-free sites in the data set are used to compute the cokriged values r_a^{cok}. We can also observe that we still have good results while the amount of MT sites with static shift increases (see cases d to a). This illustrates the importance of a priori information for the correction.

COPROD-2S2: A 2D SYNTHETIC EXAMPLE

An application of the static shift correction method has been performed on the synthetic 2D MT data set COPROD-2S2. This data set has been provided by Ivan M. Varentsov (Varentsov, 1998) to test the removal of the static shift effect using 2D inversion programs. This data set is available for download at the MTNET web site (url: http://www.mtnet.info/).

MT data were computed at 35 (N) sites and at 8 (M) periods ranging from 1 to 3000 s. Some noise, outliers, and static shifts have been added to the original data set. However, the initial model and the static shift for each MT site are unknown. Here, we present results for both the transverse electric (TE) and transverse magnetic (TM) modes. Comparing the pseudosections of the measured phase and apparent resistivity (Figure 6a and b for TE, and Figure 6g and h for TM), we can delineate at least three anomalous zones, one identified as an anomalous increase of ρ_a between 500 and 515 km, and the two others showing a decrease of ρ_a, one between 520 and 525 km and the other between 535 and 545 km.

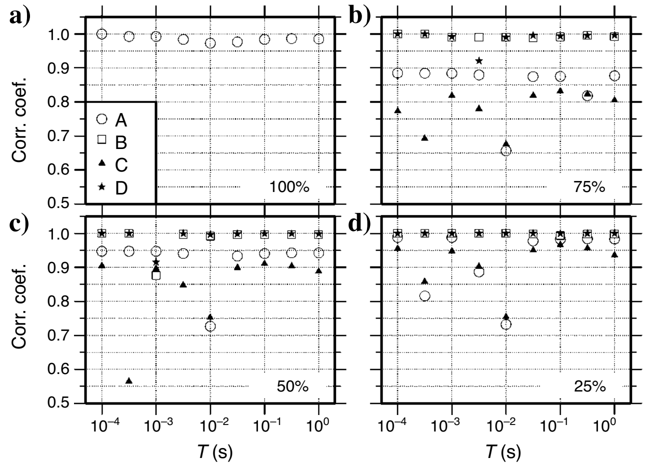

Figure 5. Graphs presenting the correlation between the static shift solution estimated at each period and the original (input) static shift. Solutions for different amounts of MT sites affected by static shifts (from 100% to 25%) are shown on graphs (a) to (d). The different solutions of the estimated static shift sta.cok according to the amount of sites used to compute the experimental variogram of r_a^{obs} and the cokriged values r_a^{cok} are presented with symbols (see definition in Figure 4).

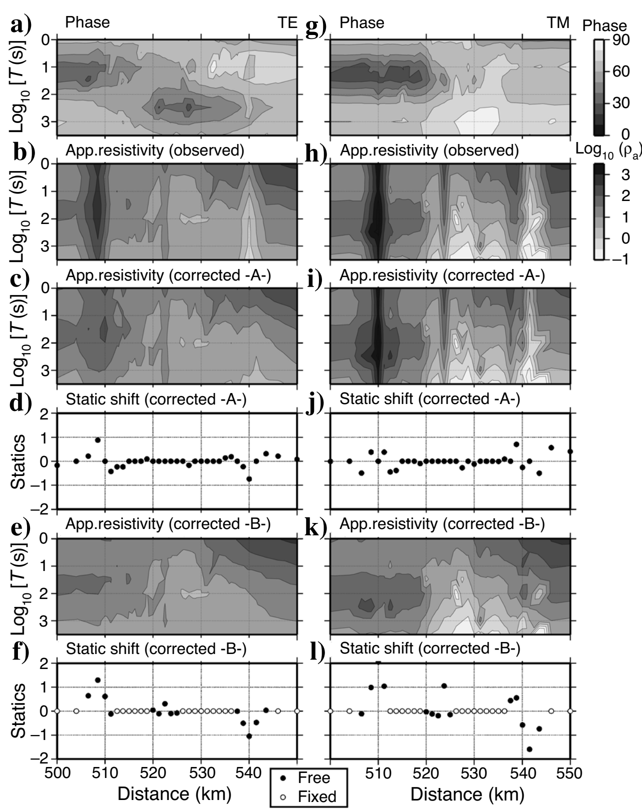

Figure 6. Results of cases A and B on the COPROD-2S2 data set for the TE and the TM modes. Top to bottom: pseudosections of the observed phase (a and g) and apparent resistivity (b and h); corrected apparent resistivity pseudosections (case A: c and i; case B: e and k) using computed staticshift data set (case A: d and j; case B: f and l).

A first estimate of the static shifts was computed for all the MT sites without any constraint (case A) and for each period. The static-shift solution presenting the highest average correlation with the other solutions is retained as the final estimate. The static shift data set for TE ($T = 3$ s) and TM ($T = 1$ s) modes is presented in Figure 6d and j, and the corrected TE and TM apparent resistivity pseudsections are shown in Figure 6c and i, respectively. Corrections applied to the apparent resistivities are mainly located near the ends of the profile, as it was suggested by our observations on the MT pseudosections. There is also no clear evidence for static shifts in the middle of the profile, but one can observe small variations near positions 520 and 528 km (Figure 6d and j). Furthermore, we can observe that the final correction has removed some part of the anomalous increase or decrease of ρ_a, but it is clear that TM apparent resistivities are still affected by a static shift.

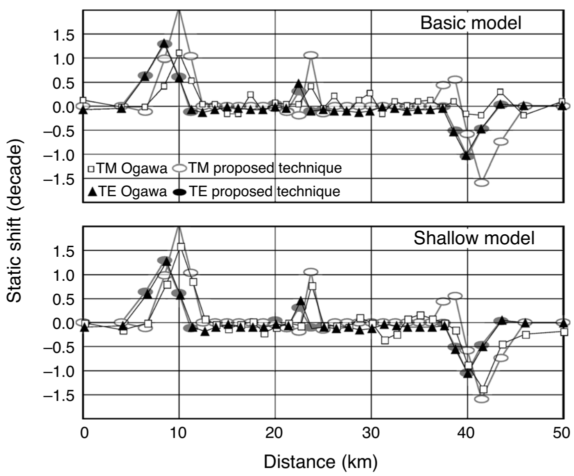

Figure 7. Distribution of static shift for the basic model (top) and for the shallow horizontal model (bottom) estimated by Ogawa (1999) for the COPROD-2S2 data set. TM- and TE-mode static shifts are shown by white squares and black triangles, respectively (redrawn from Ogawa, 1999). Results of case *B* (see Figure 6) are overprinted on both graphics using white and black ovals for the TM and TE mode, respectively.

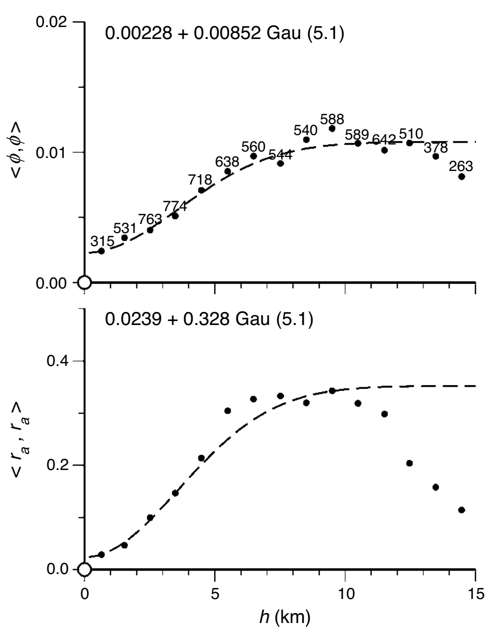

Figure 8. Experimental variograms and models (top: ϕ; bottom: r_a) at $T = 0.0087$ s. The number of pairs ($N(h)$) are shown as labels on the phase plot. Solid lines are the models (see equation on each plot).

Results of this first analysis and our observations on the MT pseudosections were used to delineate three zones where sites are potentially affected by some static shift. Those zones are located at the western, central, and eastern part of the profile. Static shifts of MT sites within each zone were then left free while the static shifts for all the other sites were fixed to $s = 0$. A new set of static shift values for each period was then computed using that constraint. Note here that tests have been performed using both B and D strategies (see Figure 4 and previous section for explanation), but only results for the B case is presented here because both B and D cases give similar results.

The static shift data set for both TE and TM modes, case B for $T = 3$ s, is presented in Figure 6f and l, and the corrected pseudosections in Figure 6e and k, respectively. Here, we observe that the large variations of ρ_a between 500 and 515 km, between 535 and 545 km, and near 525 km have been removed. Furthermore, final static shifts computed here are also consistent with those computed during the inversion (2D) of the data by Ogawa (1999) (Figure 7). In the TM mode, the static shifts estimated by our approach are slightly different from those of Ogawa, especially for the basic model. However, the static shift in the TE mode is almost identical for both methods. These results clearly demonstrate that this method can be applied on 2D data sets.

LAS CAÑADAS CALDERA (TENERIFE, CANARY ISLANDS)

Here, we present the application of our static correction technique to a 3D audio-magnetotelluric (AMT) data set acquired over Las Cañadas Caldera (Tenerife, Canary Islands) by Coppo et al. (2004). The main objectives of their project were to reveal the shallow caldera structure of the volcanic island and to estimate the depth to the impermeable floor (hydrothermalized lavas) to gain valuable information on the geometry of local aquifers. The AMT data were acquired at 133 sites. We have used the apparent resistivities and phases estimated for 17 periods between 0.0021 s and 0.2738 s (i.e., frequencies between 486.4 and 3.65 Hz).

Experimental variograms (and cross variograms) were estimated and modeled at each period. An example of the experimental variogram for the phase ϕ and for the logarithm of the apparent resistivity r_a for $T = 0.0087$ s is presented in Figure 8. Models that best fit those variograms are also displayed in the figure.

Results from the estimation of the XY static shift for the 133 AMT sites are presented in Figure 9a. Here, static shift for all the AMT sites were not constrained (case A). The mean and standard deviation estimated at each AMT site using all the periods are shown in Figure 9b. There is a proportional effect between the (absolute) mean level of the static shift and the standard deviation obtained with the various periods. This kind of proportional effect occurs commonly for quantities having skewed distributions. These results clearly show that only a few sites seem to be affected by static shift. Furthermore, we can observe relatively small errors for the static shift estimates at most of the sites, which suggests that dispersion over the periods is not very large.

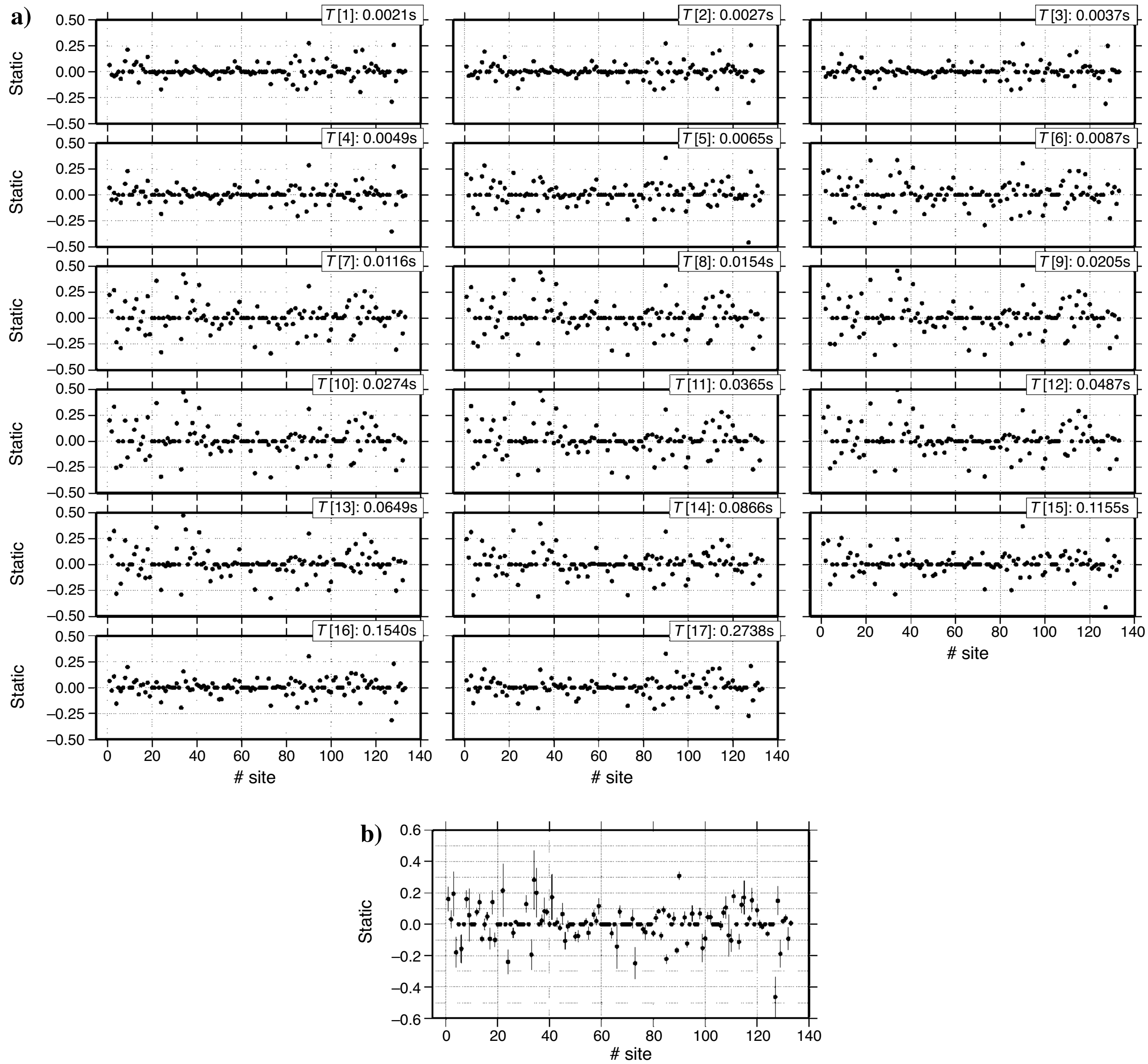

Figure 9. Canary Island data: (a) Estimates of the XY static shift parameters at each site and for each period. (b) Mean and standard deviation for the XY static shift parameters estimated at each AMT site using results in (a).

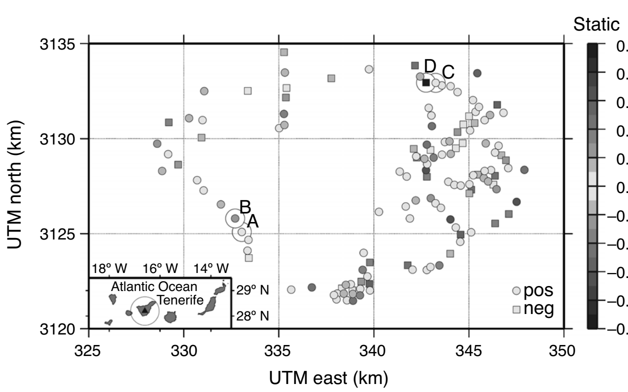

Figure 10. XY static shift estimated at each AMT site. Positive values are presented by circle symbols, and negative values, by squares. Removal of the static shift for sites [A,B] and [C,D] are presented in Figure 11.

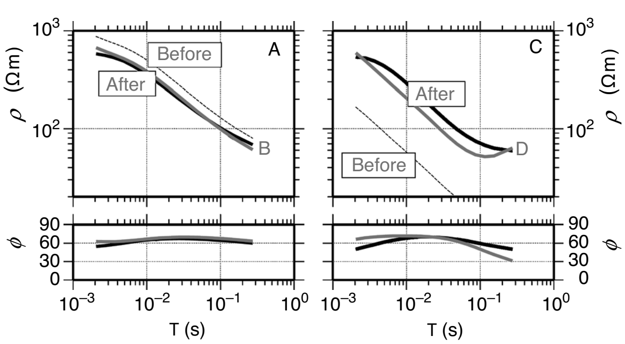

Figure 11. XY sounding curves at sites [A,B] and [C,D]: before and after static shift correction. Sites A and C (plain black line) display no static; B and D after static shift correction (plain light gray line) are similar to A and C, respectively. Dotted lines are for B and D soundings before correction.

The static shift solution for $T = 0.0087$ s is retained for the final static shift correction because it presents the highest average correlation with the other solutions. The static shift coefficients for each AMT site are presented in Figure 10 using circle and square symbols to differentiate positive (or nil) and negative values, respectively.

The XY sounding curves for sites A and B and for sites C and D are displayed before and after correction for the static shift in Figure 11. Locations for those sites are shown in Figure 10. In both cases, we observe that the correction has reduced the apparent resistivities of site B (respectively, D) to the level observed at site A (respectively, C). Sites A and C are unaffected by static shift.

CONCLUSIONS

We have presented in this paper a novel approach to estimate the static shifts affecting AMT/MT sites. The method is based on the similarities of spatial structure of the phases and apparent resistivities. The cokriging method is used to compute at each period a new estimate of the apparent resistivity using the spatial distribution of the observed phase. The method is based on covariance models of the apparent phases and resistivities; therefore, their estimates are dependent on the number of MT sites available. The method is applicable whenever this number is high. A minimum of 30 MT sites is recommended.

Analysis of a 3D synthetic example clearly shows that a priori information is needed to refine the estimation in case of bias in the static shift distribution. In particular, very good results are found when only sites not affected by static shift were used to compute the (cross) variograms and were used in the cokriging system. The method appears to be well adapted for 3D MT surveys; however, its application to 2D MT surveys is also possible if sufficient MT sites are recorded (see the COPROD-2S2 example).

ACKNOWLEDGMENTS

The authors thank NSERC grant CRDPJ 223546, Phoenix Geophysics, and Falconbridge Ltd. for financial support. 3D forward modeling was performed with the processing facilities of the ETOILE (CFI) project. The authors thank Nicolas Coppo (University of Neuchâtel) for providing us with the AMT data set from Las Cañadas Caldera (Tenerife, Canary Islands). The authors also thank the reviewers and associate editor for their detailed comments, which helped to improve the final manuscript.

REFERENCES

Andrieux, P., and W. E. Wightman, 1984, The so-called static corrections in magnetotelluric measurements: 54th Annual International Meeting, SEG, Abstracts, 43–44.

Bahr, K., 1988, Interpretation of the magnetotelluric impedance tensor: Regional induction and local telluric distortion: Journal of Geophysics, **62**, 119–127.

Berdichevsky, M. N., L. L. Vanyan, V. A. Kuznetsov, V. T. Levadny, M. M. Mandelbaum, G. P. Nechaeva, B. A. Okulessky, P. P. Shilovsky, and I. P. Shpak, 1980, Geoelectric model of the Baikal region: Physics of the Earth and Planetary Interiors, **22**, 1–11.

Chilès, J. P., and P. Delfiner, 1999, Geostatistics: Modeling special uncertainty: John Wiley & Sons, Inc.

Coppo, N., P. A. Schnegg, W. Heise, and P. Falco, 2004, Subsurface study of the Las Cañadas Caldera (Tenerife, Canary Islands) using the audiomagnetotelluric method: Presented at the 17th Workshop on Electromagnetic Induction in the Earth.

Cressie, N., 1993, Statistics for spatial data (rev. ed.): John Wiley & Sons, Inc.

deGroot-Hedlin, C., 1991, Removal of static shift in two dimensions by regularized inversion: Geophysics, **56**, 2102–2106.

Fischer, G., and P. A. Schnegg, 1980, The dispersion relations of the magnetotelluric response and their incidence on the inversion problem: Geophysical Journal of the Royal Astronomical Society, **62**, 661–673.

Jones, A. G., 1988, Static shift of magnetotelluric data and its removal in sedimentary basin environment: Geophysics, **53**, 967–978.

Lajaunie, C., and R. Béjaoui, 1991, Sur le krigeage des functions complexes: Technical Report N-23/91/G, Centre de Géostatistique, Ecole de Mines de Paris.

Langlois, P., L. Bolduc, and M. Chouteau, 1996, Probability of occurrence of geomagnetic storms based on a study of the distribution of the electric field amplitudes measured in Abitibi, Québec, in 1993–94: Journal of Geomagnetism and Geoelectricity, **48**, 1033–1041.

Ledo, J., A. Gabàs, and A. Marcuello, 2002, Static shift levelling using geomagnetic transfer functions: Earth Planets and Space, **54**, 493–498.

Mackie, R. L., J. T. Smith, and T. R. Madden, 1994, Three-dimensional electromagnetic modeling using finite difference equations: The magnetotelluric example: Radio Science, **29**, 923–935.

Marcotte, D., 1991, Cokriging with Matlab: Computer and Geosciences, **17**, 1265–1280.

Meju, M. A., 1996, Joint inversion of TEM and distorted MT soundings: Some effective practical considerations: Geophysics, **61**, 56–65.

Nyquist, J. E., W. E. Doll, R. K. Davis, and R. A. Hopkins, 1996, Cokriging surface topography and seismic refraction data for bedrock topography: Journal of Environmental and Engineering Geophysics, **1**, 67–74.

Ogawa, Y., 1999, Constrained inversion of COPROD-2S2 data set using model roughness and static shift norm: Earth Planets and Space, **51**, 1145–1151.

———, 2002, On two-dimensional modeling of magnetotelluric field data: Surveys in Geophysics, **23**, 251–273.

Ogawa, Y., and T. Uchida, 1996, A two-dimensional magnetotelluric inversion assuming Gaussian static shift: Geophysical Journal International, **126**, 69–76.

Orange, A. S., 1989, Magnetotelluric exploration for hydrocarbon: Proceedings of the IEEE, 287–317.

Pellerin, L., and G. W. Hohmann, 1990, Transient electromagnetic inversion: A remedy for magnetotelluric static shifts: Geophysics, **55**, 1242–1250.

Rodi, W., and R. Mackie, 2001, Nonlinear conjugate gradients algorithm for 2D magnetotelluric inversion: Geophysics, **66**, 174–187.

Schultz, A., R. D. Kurtz, A. D. Chave, and A. G. Jones, 1993, Conductivity discontinuities in the upper mantle beneath a stable craton: Geophysical Research Letters, **20**, 2941–2944.

Singer, B. S., 1992, Correction for distortions of magnetotelluric fields: Limits of validity of the static approach: Surveys in Geophysics, **13**, 309–340.

Smith, J. T., and J. R. Booker, 1991, Rapid inversion of two- and three-dimensional magnetotelluric data: Journal of Geophysical Research, **96**, 3905–3922.

Sternberg, B. K., J. C. Washburne, and L. Pellerin, 1988, Correction for the static shift in magnetotellurics using transient electromagnetic soundings: Geophysics, **53**, 1459–1468.

Torres-Verdín, C., and F. X. Bostick, 1992, Principles of spatial surface electric field filtering in magnetotellurics: Electromagnetic array profiling (EMAP): Geophysics, **57**, 603–622.

Tournerie, B., and M. Chouteau, 1998, Deep conductivity structure in Abitibi using long dipole magnetotelluric measurements: Geophysical Research Letters, **25**, 2317–2320.

———, 2002, Analysis of magnetotelluric data along the Lithoprobe seismic line 21 in the Blake River Group, Abitibi, Canada: Earth Planets and Space, **54**, 575–589.

Varentsov, I. M., 1998, 2D synthetic data sets (COPROD-2S) to study MT inversion techniques: Presented at the 14th Workshop on Electromagnetic Induction in the Earth.

Vozoff, K., 1991, The magnetotelluric method, *in* M. N. Nabighian, ed., Electromagnetic methods in applied geophysics Part B, Vol. 2: SEG, Investigation in geophysics 3, 641–711.

Wackernagel, H., 2003, Multivariate geostatistics: An introduction with applications, 3rd ed.: Springer-Verlag.

Wu, N., J. R. Booker, and J. T. Smith, 1993, Rapid two-dimensional inversion of COPROD2 data: Journal of Geomagnetism and Geoelectricity, **45**, 1073–1087.

Zhang, P., M. Chouteau, M. Mareschal, R. Kurtz, and C. Hubert, 1995, High-frequency magnetotelluric investigation of crustal structure in northern central Abitibi, Quebec, Canada: Geophysical Journal International, **120**, 406–418.